Amino Acids (2009) 37:523–530
DOI 10.1007/s00726-009-0256-5

ORIGINAL ARTICLE

Site-directed mutagenesis and computational study of the Y366 active site in *Bacillus subtilis* protoporphyrinogen oxidase

Lu Sun · Xin Wen · Ying Tan · Heyang Li · Xing Yang · Yuefang Zhao · Baifan Wang · Qiongyao Cao · Congwei Niu · Zhen Xi

Received: 27 September 2008 / Accepted: 2 February 2009 / Published online: 6 March 2009

Abstract Protoporphyrinogen IX oxidase (PPO), the last common enzyme of heme and chlorophyll biosynthesis, catalyses the oxidation of protoporphyrinogen IX to protoporphyrin IX, with FAD as cofactor. Among PPO, *Bacillus subtilis* PPO (*bs*PPO) is unique because of its broad substrate specificity and resistance to inhibition by diphenylethers. Identification of the activity of *bs*PPO would help us to understand the catalysis and resistance mechanisms. Based on the modeling and docking studies, we found that Y366 site in *bs*PPO was adjacent to substrate and FAD. In order to evaluate the functional role of this site, three mutants Y366A Y366E and Y366H were cloned and kinetically characterized. The efficiency of catalysis for Y366A and Y366H reduced to 10% of the wild-type enzyme's activity, while Y366E just retained 1%. Y366E shows large resistance ($K_i = 153.94$ μM) to acifluorfen. Molecular docking was carried out to understand the structure and functional relationship of PPO. The experimental results from the site-directed mutagenesis are consistent with the computational studies. The residue at position 366 is seemed to be responsible for substrate binding and catalysis and involved in herbicide resistance of *bs*PPO.

Keywords Kinetics · Molecular docking · Protoporphyrinogen oxidase · Site-directed mutagenesis

Abbreviations

PPO	Protoporphyrinogen oxidase
*bs*PPO	*Bacillus subtilis* PPO
*mt*PPO	Mitochondrial tobacco PPO
*mx*PPO	*Myxococcus xanthus* PPO
protogen	Protoporphyrinogen IX
proto	Protoporphyrin IX
FAD	Flavin adenine dinucleotide
AF	Acifluorfen
VP	Variegate porphyria
DPEs	Diphenylethers
SDS-PAGE	Sodium dodecyl sulfate polyacrylamide gel electrophoresis

Introduction

Protoporphyrinogen oxidase (PPO, EC 1.3.3.4), a member of the superfamily of flavin adenine dinucleotide (FAD)-containing proteins, is the last enzyme in the common tetrapyrrole biosynthesis pathway just before the pathway branches toward chlorophyll and heme synthesis. PPO provides protoporphyrin IX (proto) for both Mg chelatase and ferrochelatase at the branchpoint by catalyzing the oxidation of the protoporphyrinogen IX (protogen) (Scheme 1), which leads to chlorophyll and heme, respectively. For green plants, inhibition of PPO leads to rapid bleaching and desiccation of photosynthetically active tissues. These characteristics make PPO an excellent target for light-dependent peroxidizing herbicides such as diphenylether acifluorfen (Lermontova et al. 1997). Apart from the

Electronic supplementary material The online version of this article (doi:10.1007/s00726-009-0256-5) contains supplementary material, which is available to authorized users.

L. Sun · X. Wen · Y. Tan · H. Li · X. Yang · Y. Zhao · B. Wang · Q. Cao · C. Niu · Z. Xi (✉)
State Key Laboratory of Elemento-Organic Chemistry, Department of Chemical Biology, Nankai University, 300071 Tianjin, China
e-mail: zhenxi@nankai.edu.cn

economic interest because of potential applications in agriculture and biotechnology, the intense study of PPO may also contribute to the development of effective treatments for human porphyria diseases. In humans, a defective PPO results in the dominantly inherited disorder variegate porphyria (VP), the most obvious sign being the light sensitivity of the patient's skin (Harper and Wahlin 2007). The direct effect of some mutations on PPO activity in VP has been investigated (Meissner et al. 1996). However, in contrast to the extensive identification of PPO mutations in VP patients and a great deal of investigation about inhibitors of PPO, the mechanism of oxidation reaction catalyzed by PPO is poorly understood at the molecular level despite years of intense study. Reorganization of residues that appear important for substrate binding and/or catalysis is critical for yielding insights into the mechanistic aspects of PPO. Recently, Heinemann et al. (Heinemann et al. 2007; Koch et al. 2004) have used a model based on the solved crystal structure of mitochondrial tobacco PPO (*mt*PPO) to generate variant proteins carrying amino acid residue exchanges in the corresponding positions of the active site domain. Though functional definition of the *mt*PPO substrate binding site was given, the mechanism of oxidation reaction catalyzed by PPO needs more detailed research.

Of the PPO studied to date, *Bacillus subtilis* PPO (*bs*PPO) is apparently unique from others. *bs*PPO is present in the soluble cytoplasmic fraction and has broad substrate specificity (Hansson and Hederstedt 1994), which is not inhibited by acifluorfen (AF), one of the typical diphenylether (DFE) herbicides (Choi et al. 1998; Matringe et al. 1989). Due to resistance of *bs*PPO against DFE herbicide, its gene has been used for developing herbicide resistant transgenic plants (Matringe et al. 1989; Choi et al. 1998; Lee et al. 2000; Il Jung and Kuk 2007). Unfortunately, the resistance of *bs*PPO has not been completely understood at the molecular level (Jeong et al. 2003).

Because of its unique properties *bs*PPO is an ideal model for studying the mechanistic aspects of PPO. Based on the homology model and docking results, the Y366 site of *bs*PPO was adjacent to substrate/inhibitor and FAD. Therefore, we used site-directed mutagenesis method in *bs*PPO at this site to construct different mutants, which were purified and kinetically characterized. Computational studies were carried out to understand the PPO structure and functional relationship.

Materials and methods

Materials

Protoporphyrin IX was purchased from Tokyo Kasei Kogyo Co., Ltd (Tokyo, Japan), which was dissolved in 10 mM KOH containing 20% (v/v) ethanol to make a stock solution (1.5 mM). FAD was obtained from Sigma Chemical Co. (St. Louis, Missouri, USA). Restriction enzymes and T4 DNA ligase were purchased from Takara (Shiga, Japan). The nickel affinity column was purchased from QIAGEN (Hilden, Germany). Dithiothreitol (DTT) was obtained from Ding Guo Company (Beijing, China). All other chemicals were of the highest grade commercially available.

Site-directed mutagenesis and expression of the recombinant enzyme

A fragment containing the full-length coding region for the *bs*PPO was generated by PCR with *Bacillus subtilis* genomic DNA as template. The purified PCR product was digested by *Bam*HI/*Hin*dIII mixture, and then ligated into the multiple cloning site of pQE 30UA vector. The constructed plasmid was used as a template for site-directed mutagenesis with the PCR-based method. Three oligonucleotides 5′-TGCTTCGGGCA**GCT**GTCGGAAAAGC-3′ (Tyrosine^{366} → Alanine), 5′-TGCTTCGGGCA**GAA**GTC GGAAAAGC-3′ (Tyrosine^{366} → Glutamic acid) and

Scheme 1 Protoporphyrinogen oxidase reaction

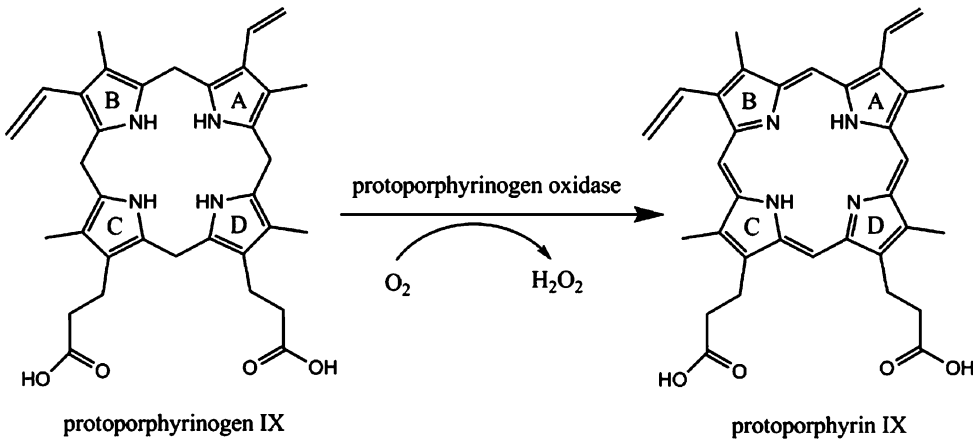

protoporphyrinogen IX protoporphyrin IX

5′-TGCTTCGGGCA**CAT**GTCGGAAAAGC-3′ (Tyrosine^{366} → Histidine) were designed for the Y366A, Y366E and Y366H mutation, respectively. The mutated plasmids were generated by the same process according to the wild-type plasmid. Recombinant proteins were expressed in *E. coli* strain XLl-Blue as inclusion bodies by the use of the original or mutated pQE-PPO plasmids. The expression and purification of the recombinant protein were carried out by similar methods described previously for a cloned PPO from the aerobic bacterium *B. subtilis* (Corrigall et al. 1998). All the mutations were confirmed by automated direct sequencing to ensure the absence of any erroneous mutations.

Substrate preparation

Protoporphyrinogen IX was prepared by reducing 0.2 mM protoporphyrin IX in KOH/EtOH (20%) with freshly prepared 3% sodium amalgam (Brenner and Bloomer 1980) under a stream of nitrogen in a fume hood. The resultant protoporphyrinogen IX solution was filtered under nitrogen gas, adjusted to pH 8.0 by 20% phosphoric acid solutions and used immediately or stored at −80°C.

Enzyme assay for kinetic analysis

Protoporphyrinogen IX oxidase activity was assayed by measuring the constant velocity of formation of proto from protogen using a 96-well plate with the continuous fluorometric methods at room temperature (Meissner et al. 1986). Assay mixture (200 µl) contained 0.1 M potassium phosphate buffer (pH 7.5), 5 mM DTT, 1 mM EDTA, 0.03% Tween 80 (v/v), 0–6.5 µM protogen. The cofactor FAD was added to the assay at the saturating concentration. Nonenzymatic rates of protogen oxidation were measured by heat-denaturated enzyme (Retzlaff and Boger 1996). These values were subtracted from the documented enzymatic proto formation. Concentration of protogen was determined by the HPLC as described (Li et al. 1987).

The Michaelis–Menten constant (K_m), the maximal velocity (V_{max}) and the catalytic constant (k_{cat}) were determined by a Lineweaver–Burk plot:

$$\frac{1}{V_0} = \frac{K_m}{V_{max}}\frac{1}{[S]} + \frac{1}{V_{max}}$$

The slope rate (K) of emission intensity versus time was determined by using the linear range points. The initial reaction rate V_0 was calculated by K/K_0, where K_0 is the slope rate in the standard curve (emission intensity versus proto concentration). For the calculation of the catalytic efficiency k_{cat}, V_{max} was divided by the corresponding enzyme concentration (Shepherd and Dailey 2005). The activation constants (K_c) were determined by measuring PPO activity over a range of FAD concentrations at a saturating substrate concentration. The protein tested in this section was obtained by dilution of the elution protein in assay buffer without FAD, and the dialyzed with the assay buffer without FAD to remove the urea prior to assay.

$$V = \frac{V_{max}[\mathrm{FAD}]}{K_c + [\mathrm{FAD}]}$$

Inhibition studies were performed according to the method as described previously (Jeong et al. 2003) by using acifluorfen. The inhibition constant K_i discriminations from secondary replots of $1/V_{max}$ versus [AF], where K_m and V_{max} were the values determined in the presence of inhibitor (AF). Calculated K_i was obtained by applying the relationship below, which exists for competitive inhibition between K_i, K_m and IC_{50} at a saturating substrate concentration, S. IC_{50} was determined by measuring PPO activity over a range of inhibitor concentrations at a single substrate concentration.

$$K_i = \frac{IC_{50}}{S/K_m + 1}$$

Circular dichroism (CD)

The CD spectra of wild type and mutants (Y366E, Y366A, Y366H) were performed on a Jasco-715 spectropolarimeter, using quartz cylindrical cell of 1 mm path length. The cell compartment was continuously purged with dry N_2. All spectra were analyzed by a 3-spectrum accumulation at room temperature in 0.1 M potassium phosphate buffer (pH 7.5), containing 5 mM DTT, 1 mM EDTA, 0.03% Tween 80 (v/v). The data were showed in Fig. 4.

Homology modeling

To obtain the 3D model of *bs*PPO, multiple sequence alignment was carried out using the software ClustalW (http://www.ebi.ac.uk/clustalw/). The amino acid sequences in the multiple alignments were extracted from the SWISS-PROT and TrEMBL databases of the ExPASy Molecular Biology Server (http://www.expasy.org/sprot/), including the human PPO, *Bacillus subtilis* PPO (*bs*PPO), mitochondrial tobacco PPO (*mt*PPO), and *Myxococcus xanthus* PPO (mxPPO) (primary accession numbers P50336, P32397, O24164 and P56601, respectively). Based on the alignment produced by ClustalW (http://www.ebi.ac.uk/clustalw/), the crystal structure of *mx*PPO (PDB ID, 2IVD) (Corradi et al. 2006), with a resolution of 2.30 Å, was used as the template to model the *bs*PPO by Insight II/Homology program (Accelrys Inc., San Diego, CA, USA). A series of energy minimizations was carried out with the Discover module of Insight II (Accelrys Inc., San Diego, CA, USA) in order to relax loops and bad contacts between the nonbonded atoms.

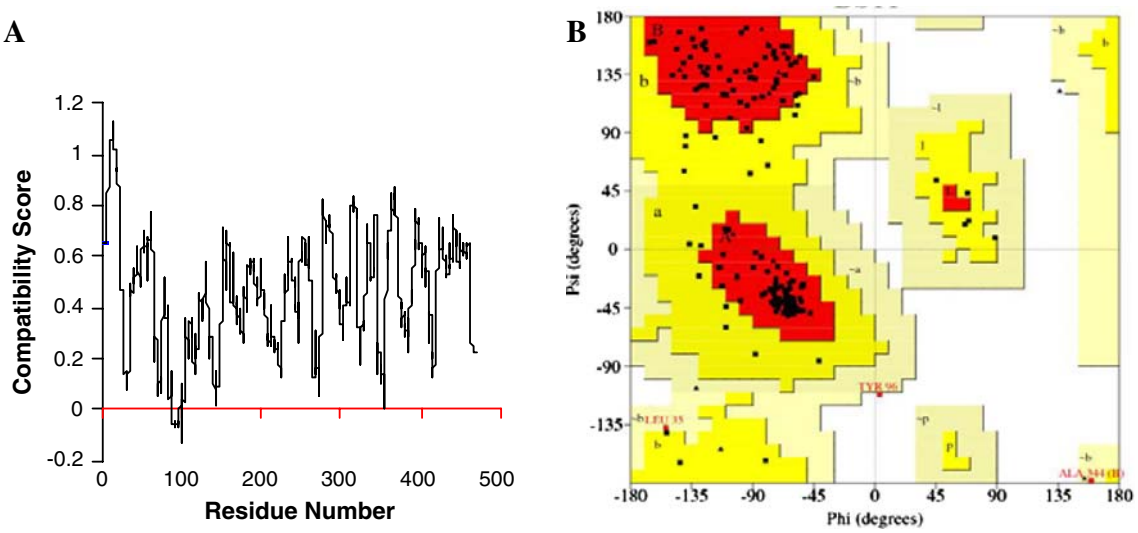

Fig. 1 **a** The 3D profiles verified results of *bs*PPO model. Residues with positive compatibility score are reasonably folded. **b** Ramachandran plot of the main-chain dihedral angles (Φ, Ψ) for *bs*PPO model

The generated models were checked using Profile-3D (Bowie et al. 1991) and PROCHECK (Laskowski et al. 1993) programs, and the structure with the best stereochemical and folding qualities was retained.

Preparation of substrate and receptor molecules for docking

The initial structures of protogen for the docking studies were constructed by making a series of ring conformations using molecular mechanics with a random search routine, implemented in Sybyl 6.9 (Tripos, Inc.) in the following manner: the maximum number of search iterations was set to 5,000, with a 30 kcal/mol energy cutoff, and 0.2 rms threshold. The structure energy minimization was performed using the standard Tripos molecular mechanics force field (Clark et al. 1989) and Gasteiger–Marsili charges (Mortier et al. 1985), with a 0.001 kcal/mol energy gradient convergence criterion. The structure of *bs*PPO by homology modeling was used in the docking experiments. This macromolecule was prepared by the Insight II program package using the CVFF force field.

Docking simulations

Docking experiments were carried out using the Lamarckian genetic algorithm implemented (LAG) in the automated docking program Autodock, version 3.0.5 (Morris et al. 1998). A total of 18 conformers of protogen obtained from conformational analysis, representing 18 conformations of the tetrapyrrole ring of the protogen, were docked into the active site of *bs*PPO, respectively. All active torsions of the protogen were selected to be fully flexible during the docking experiment. Atomic affinity and electrostatic grid maps using AutoGrid 3.0 (Morris et al. 1998) were computed for each atom type in protogen. A total of 500 LGA docking runs were performed for each starting structure. The results for all 18 tasks were combined and analyzed. In analyzing the docked conformations, the clustering tolerance of the root mean square positional deviation was 2.0 Å.

Results and discussion

Homology model and proposed 3D structure of *bs*PPO

Figure 1a shows the structural statistics of *bs*PPO calculated using the PROCHECK program (Laskowski et al. 1993). A Ramachandran plot demonstrates that 98% of the residues are found in the allowed regions, except the region N89-V97 (Fig. 1b). These residues, however, are located far from the putative substrate binding site of *bs*PPO, which would not be expected to show significant influence on our following study. The model of the *bs*PPO is shown in ribbon diagram form (Fig. 2a). Docking experiments were carried out using the conformations of the protogen into the active site of *bs*PPO. The most favorable binding mode of docking result for protogen in *bs*PPO was shown in Fig. 2b. The amino acids located within 4 Å of the substrate are displayed (Fig. S2). It is noted that Y366 in *bs*PPO which was equal to F392 in *mt*PPO was adjacent to substrate and FAD. We suggest that the residue at position Y366 might be responsible either directly or indirectly for substrate binding and catalysis. Based on the homology model, the residues surrounding the Y366 are charged or

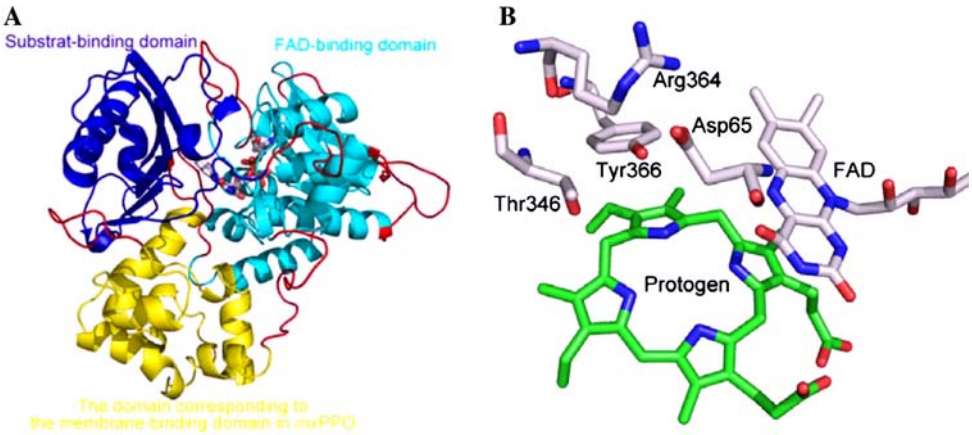

Fig. 2 **a** The model of the *bs*PPO is shown in ribbon diagram form. Regions where the backbone conformation has the greatest uncertainty, because of deletions/insertions relative to *mx*PPO, are shown as *red coils*. Bound FAD (*in stick*) is also shown. The FAD-binding domain is shown in *cyan*, the domain corresponding to the membrane-binding domain in mxPPO is shown in *yellow*. **b** Tyrosine366 of *bs*PPO, FAD and the modeled substrate protoporphyrinogen IX region around the residue based on the computational studies (Color figure online)

polar such as D65, T346, and R364 (Fig. 2b). In order to investigate the influence of charged residues in the 366 site based on site-directed mutagenesis, three mutants (Y366A for nonpolar residue, Y366E for acidic residue, Y366H for basic residue) were generated and kinetics studies herein.

Production of site-directed mutants of *bs*PPO

Based on the modeling and docking studies, any changes in Y366 site could affect the interaction between enzyme and substrate and FAD. In order to evaluate the functional role of Y366 in *bs*PPO, the residue at this site was mutated to Ala, Glu, His (Y366A, Y366E and Y366H), respectively. The mutants behaved similarly to the wild-type enzyme in SDS-PAGE (Fig. 3). The CD spectra imply that the wild-type and mutant enzymes have very similar structures (Fig. 4). Kinetic constants of enzyme activity were determined via continuous fluorescence method in comparison with wild-type *bs*PPO (Fig. 5).

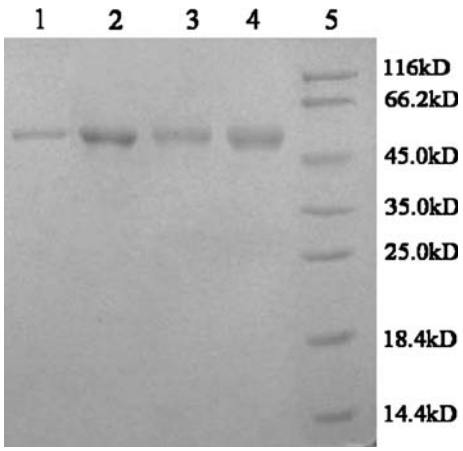

Fig. 3 SDS-PAGE of wild-type and mutated PPO proteins. Wild-type PPO (*lane 1*), and mutated proteins Y366A (*lane 2*), Y366E (*lane 3*), Y366H (*lane 4*) underwent electrophoresis on a standard 12% gel and were stained with Coomassie Brilliant Blue. Molecular mass markers (kDa) are shown in *lane 5*

Y366 site-directed mutants

The kinetic study of mutations revealed an increase of K_m and a decrease of k_{cat} compared with that of wild-type *bs*PPO (Table 1). Y366H showed significant change in K_m value (3.54 ± 0.05 μM, pH 7.5). The turn over number (k_{cat}) of mutants was less than the wild type. As a result, the catalytic efficiency (k_{cat}/K_m) of mutant Y366A and Y366H showed 10% of the wild-type enzyme activity, while Y366E just retained 1% of the activity (Fig. 6). These results showed that the negative charge of the introduced Glu influences the enzymatic properties greatly. In this study, residue Y366 of *bs*PPO is equivalent to F392 of *mt*PPO, which has been proposed to play an important role in substrate binding and catalysis by site-directed mutagenesis (Heinemann et al. 2007). In contrast with Y366E of *bs*PPO, the corresponding mutation F392E in *mt*PPO results in increasing k_{cat} value. We also found that introduction of the residue with negatively charge group cause significant change in inhibitor binding. Figure 7 shows AF inhibition of mutants of *bs*PPO, where the IC_{50} of Y366E is 617.32 μM. Though the Y366A mutation does not alter AF sensitivity, Y366E shows near five-fold larger K_i value than that of wild-type enzyme. For the *bs*PPO variant Y366H, we measured kinetic parameters of Y366H at pH 6.0 and 7.5. It was noted that Y366H exhibited a larger K_m value in pH 6.0 than in pH 7.5. However, the *mt*PPO variant F392H at pH 6.0 lead to a totally inactive enzyme

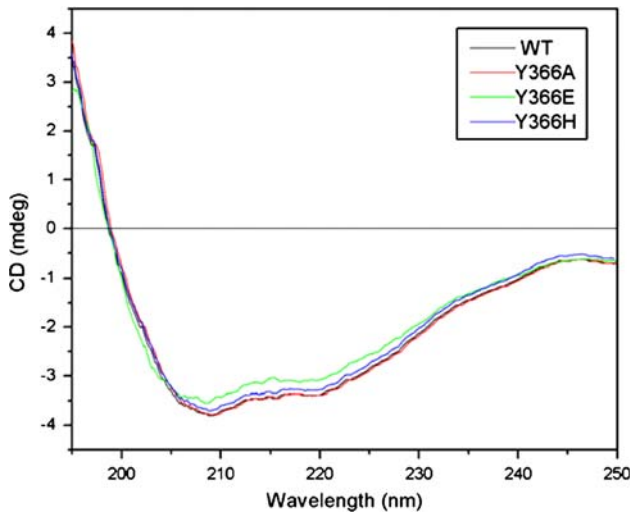

Fig. 4 CD spectra of wild type and mutant (Y366A, Y366E, Y366H) protoporphyrinogen oxidase from *Bacillus subtilis* (Color figure online)

owing to the repulsion between substrate ring A and the side chain of histidine (Heinemann et al. 2007). Cofactor FAD studies showed that the mutants had higher K_c value than that of wild-type enzyme (Table 1). This result showed that introduction of the amino acid residue with charge group or small side chain affects the proper function of FAD.

Relationship between mutagenesis data and molecular models

In order to understand enzymatic properties at the molecular level, homology modeling and automated docking with AutoDock were used to extend our knowledge of PPO mutants' structure and its relationship to function. Several interesting observations emerged by observing the residues near the Y366 in the *bs*PPO. The model revealed that the aromatic ring of the protogen is kept in position by aromatic stacking with Y366 (Fig. 2b). Base on crystal structure of the *M. xanthus* PPO (*mx*PPO) with AF (Corradi et al. 2006), it can be proposed that there would also be aromatic stacking interaction between Y366 and 2-chloro-4-trifluoromethylphenoxy moiety of AF. Therefore when the residue was replaced by Ala or Glu, the aromatic stacking interaction disappear (Fig. 2b), followed by a weaker substrate/inhibitor binding. As a result, both mutants showed increased K_m and K_i value. On the other hand, based on the model (Fig. S3), the residues surrounding the Y366 are charged or polar such as D65, T346, and R364. Glu residue at positions 366 is unfavorable due to electrostatic repulsion between the E366 and D65, and Ala residue at positions 366 is unfavorable due to interaction disappeared between the 366 and 65 sites. D65 is on

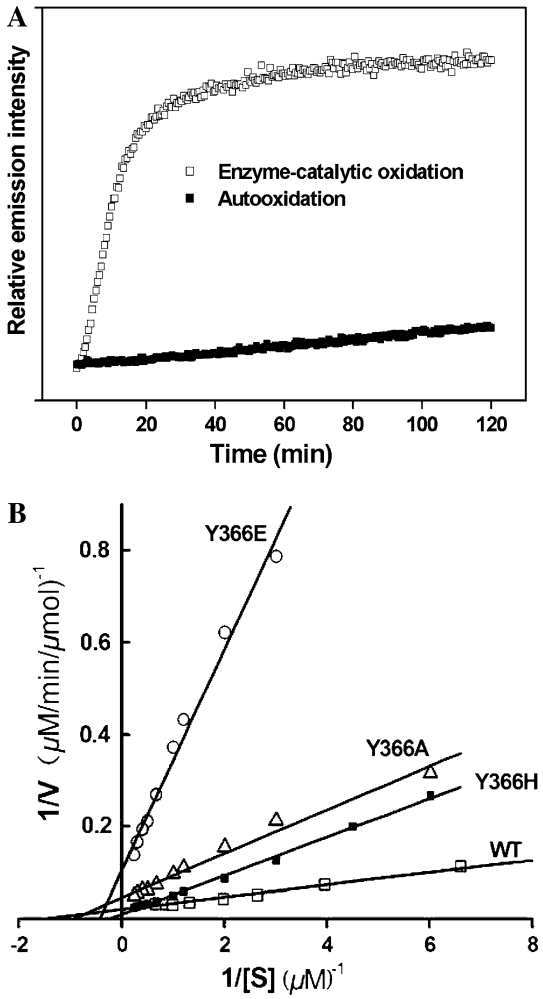

Fig. 5 **a** A typical fluorescent assay of protoporphyrin IX for kinetic study. **b** Determination of apparent Michaelis constant for *bs*PPO activities was assayed by using varying concentrations of protoporphyrinogen IX. The experimental data were fitted by Lineweaver–Burk equation as shown in *solid line*

a flexible loop; it is possible for this residue to shift when it encounters strong charge repulsion or interaction disappeared. The subtle movement might finally affect the proper function of FAD in *bs*PPO because D65 locates near FAD, which is consistent with K_c values (Table 1). In contrast with the region of Y366 in *bs*PPO, the corresponding region in the *mt*PPO is nearly hydrophobic (Fig. S3). Thus, the introduction of residue Glu in *mt*PPO in such hydrophobic environment should have a smaller electrostatic repulsion than that in *bs*PPO, resulting in a smaller effect on substrate binding and catalysis in F392E mutant (Heinemann et al. 2007).

The pKa of free imidazole ring in histidine is about 6.5, which could be modulated by its environment within the protein. Under the experimental conditions (in pH 6.0), the histidine residue is likely to support a positive charge, which might trigger repulsion between the positively

Table 1 Kinetic parameters for wild-type and mutant PPOs

	K_m (μM)	k_{cat} (min^{-1})	k_{cat}/K_m (μM^{-1} min^{-1})	K_c (μM)	IC_{50} (μM)	K_i (μM)
Wild type	0.67 ± 0.12	0.201 ± 0.008	0.299	0.23 ± 0.02	183.02 ± 32.70	32.98 ± 6.46
Y366A	1.07 ± 0.07	0.025 ± 0.001	0.023	0.74 ± 0.12	172.96 ± 43.11	28.52 ± 7.18
Y366E	2.34 ± 0.05	0.009 ± 0.001	0.003	1.18 ± 0.25	617.32 ± 111.66	153.94 ± 25.69
Y366H	3.54 ± 0.05	0.097 ± 0.001	0.027	0.49 ± 0.10	133.27 ± 18.98	53.05 ± 7.33
Y366H (pH 6.0)	4.09 ± 0.09	0.364 ± 0.002	0.088	0.30 ± 0.03	315.88 ± 30.58	126.81 ± 31.42

Data are the mean values ± SD of two separate experiments with duplicate determinations

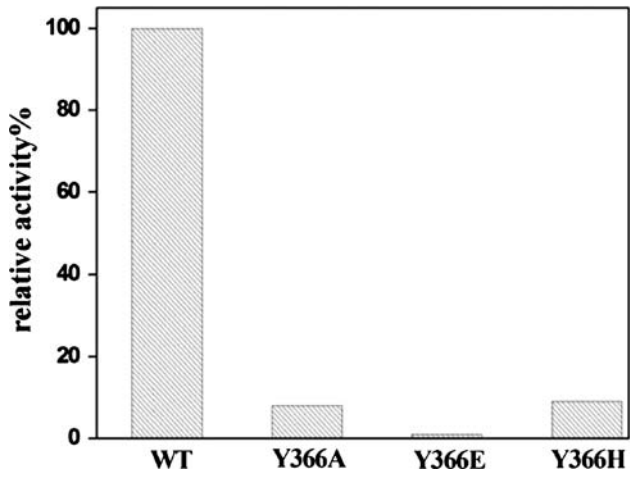

Fig. 6 Relative activity of wide type and mutants of *bs*PPO

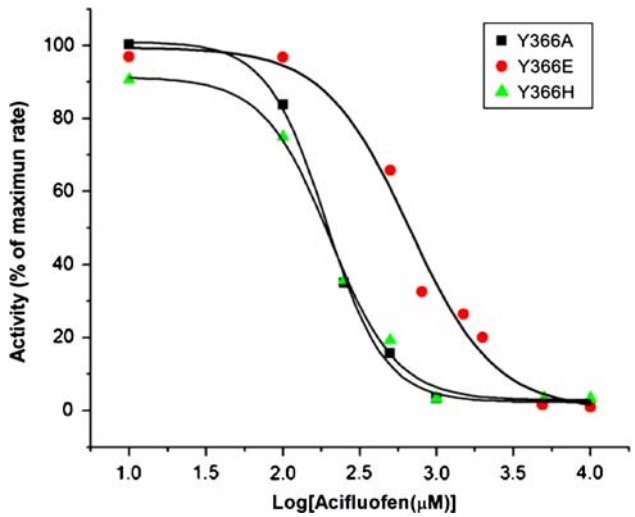

Fig. 7 *bs*PPO mutants (Y366A, Y366E, Y366H) activity curve in the presence of different concentrations of the inhibitor acifluorfen

charged histidine and substrate (Heinemann et al. 2007). However, it may be poised to electrostatically repel because of a negatively charged residue Asp65 being on the opposite of the H366, resulting the effect of mutation Y366H in *bs*PPO on substrate binding is smaller than that of mutation F392H in *mt*PPO.

Conclusion

Though PPO is a significantly important enzyme in the tetrapyrrole biosynthetic pathway, the catalysis and resistance mechanisms of PPO are poorly understood at the molecular level. Identification of the amino acid residues that are responsible for the molecular properties of PPO is important for our further understanding their functions. The homology model of *bs*PPO was successfully constructed. Based on the modeling and docking studies, Y366 in *bs*PPO was adjacent to substrate and FAD, our experimental data showed that Y366 mutants indeed cause dramatic property changes compared to that of wild-type *bs*PPO. The catalytic efficiency for Y366A and Y366H showed 10% of the wild-type enzyme activity, while Y366E just retained 1% of that activity. Y366E shows large resistance to AF. Based on experimental and computational results, a couple of points could be reasoned regarding structure–function relationship: (1) Alanine or glutamine acid instead of tyrosine residue breaches π–π stacking interaction between aromatic ring of the protogen (or 2-chloro-4-trifluoromethylphenoxy moiety of AF) and Y366, resulting the change of enzyme activity or resistance. (2) Because the residues surrounding the Y366 are charged or polar based on our model, the introduction of a charged residue (Glu, His) or an uncharged residue (Ala) at 366 site affects the surrounding electrostatic balance and finally affects the proper function of FAD in catalysis within *bs*PPO. The residue at position 366 is seemed to be responsible for substrate binding and catalysis and involved in herbicide resistance of *bs*PPO.

Acknowledgments This work was supported by the National Key Project for Basic Research of China (2003CB114403), National Natural Science Foundation of China (20432010, 20572053, 20421202, 90713011), Natural Science Foundation of Tianjin (06TXTJJC14100) and Nankai University ISC. We also thank referees of this paper for many critical discussions.

References

Bowie JU, Luthy R, Eisenberg D (1991) A method to identify protein sequences that fold into a known 3-dimensional structure. Science 253:164–170

Brenner DA, Bloomer JR (1980) Fluorometric assay for measurement of protoporphyrinogen oxidase activity in mammalian tissue. Clin Chim Acta 100:259–266

Choi KW, Han O, Lee HJ, Yun YC, Moon YH, Kim M, Kuk YI, Han SU, Guh JO (1998) Generation of resistance to the diphenyl ether herbicide, oxyfluorfen, via expression of the *Bacillus subtilis* protoporphyrinogen oxidase gene in transgenic tobacco plants. Biosci Biotech Biochem 62:558–560

Clark M, Cramer RD, Vanopdenbosch N (1989) Validation of the general-purpose Tripos 5.2 force-field. J Comput Chem 10:982–1012

Corradi HR, Corrigall AV, Boix E, Mohan CG, Sturrock ED, Meissner PN, Acharya KR (2006) Crystal structure of protoporphyrinogen oxidase from *Myxococcus xanthus* and its complex with the inhibitor acifluorfen. J Biol Chem 281:38625–38633

Corrigall AV, Siziba KB, Maneli MH, Shephard EG, Ziman N, Dailey TA, Dailey HA, Kirsch RE, Meissner PN (1998) Purification of and kinetic studies on a cloned protoporphyrinogen oxidase from the aerobic bacterium *Bacillus subtilis*. Arch Biochem Biophys 358:251–256

Hansson M, Hederstedt L (1994) *Bacillus subtilis* Hem Y is a peripheral membrane-protein essential for protoheme-IX synthesis which can oxidize coproporphyrinogen-III and protoporphyrinogen-IX. J Bacteriol 176:5962–5970

Harper P, Wahlin S (2007) Treatment options in acute porphyria, porphyria cutanea tarda, and erythropoietic protoporphyria. Curr Treat Opt Gastroenterol 10:444–455

Heinemann IU, Diekmann N, Masoumi A, Koch M, Messerschmidt A, Jahn M, Jahn D (2007) Functional definition of the tobacco protoporphyrinogen IX oxidase substrate-binding site. Biochem J 402:575–580

Il Jung H, Kuk YI (2007) Resistance mechanisms in protoporphyrinogen oxidase (PROTOX) inhibitor-resistant transgenic rice. J Plant Biol 50:586–594

Jeong E, Houn T, Kuk Y, Kim ES, Chandru HK, Baik M, Back K, Guh JO, Han O (2003) A point mutation of valine-311 to methionine in *Bacillus subtilis* protoporphyrinogen oxidase does not greatly increase resistance to the diphenyl ether herbicide oxyfluorfen. Bioorg Chem 31:389–397

Koch M, Breithaupt C, Kiefersauer R, Freigang J, Huber R, Messerschmidt A (2004) Crystal structure of protoporphyrinogen IX oxidase: a key enzyme in haem and chlorophyll biosynthesis. EMBO J 23:1720–1728

Laskowski RA, Macarthur MW, Moss DS, Thornton JM (1993) Procheck—a program to check the stereochemical quality of protein structures. J Appl Cryst 26:283–291

Lee HJ, Lee SB, Chung JS, Han SU, Han O, Guh JO, Jeon JS, An G, Back K (2000) Transgenic rice plants expressing a *Bacillus subtilis* protoporphyrinogen oxidase gene are resistant to diphenyl ether herbicide oxyfluorfen. Plant Cell Phys 41:743–749

Lermontova I, Kruse E, Mock HP, Grimm B (1997) Cloning and characterization of a plastidal and a mitochondrial isoform of tobacco protoporphyrinogen IX oxidase. Pro Nat Acad Sci USA 94:8895–8900

Li F, Lim CK, Peters TJ (1987) An HPLC assay for protoporphyrinogen oxidase activity in rat-liver. Biochem J 243:863–866

Matringe M, Camadro JM, Labbe P, Scalla R (1989) Protoporphyrinogen oxidase as a molecular target for diphenyl ether herbicides. Biochem J 260:231–235

Meissner PN, Day RS, Moore MR, Disler PB, Harley E (1986) Protoporphyrinogen oxidase and porphobilinogen deaminase in variegate porphyria. Eur J Clin Invest 16:257–261

Meissner PN, Dailey TA, Hift R, Ziman M, Corrigall AV, Roberts AG, Meissner DM, Kirsch RE, Dailey HA (1996) A R59W mutation in human protoporphyrinogen oxidase results in decreased enzyme activity and is prevalent in South Africans with variegate porphyria. Nat Gene 13:95–97

Morris GM, Goodsell DS, Halliday RS, Huey R, Hart WE, Belew RK, Olson AJ (1998) Automated docking using a Lamarckian genetic algorithm and an empirical binding free energy function. J Comput Chem 19:1639–1662

Mortier WJ, Vangenechten K, Gasteiger J (1985) Electronegativity equalization—application and parametrization. J Am Chem Soc 107:829–835

Retzlaff K, Bőger P (1996) An endoplasmic reticulum plant enzyme has protoporphyrinogen IX oxidase activity. Pest Biochem Physiol 54:105–114

Shepherd M, Dailey HA (2005) A continuous fluorimetric assay for protoporphyrinogen oxidase by monitoring porphyrin accumulation. Anal Biochem 344:115–121